Chimeras with uniformly distributed heterogeneity: two coupled populations

Carlo R. Laing*
School of Natural and Computational Sciences, Massey University,
Private Bag 102-904 North Shore Mail Centre, Auckland, New Zealand
(Dated: January 29, 2022)

Chimeras occur in networks of two coupled populations of oscillators when the oscillators in one population synchronise while those in the other are asynchronous. We consider chimeras of this form in networks of planar oscillators for which one parameter associated with the dynamics of an oscillator is randomly chosen from a uniform distribution. A generalisation of the approach in [C.R. Laing, Physical Review E, **100**, 042211, 2019], which dealt with identical oscillators, is used to investigate the existence and stability of chimeras for these heterogeneous networks in the limit of an infinite number of oscillators. In all cases, making the oscillators more heterogeneous destroys the stable chimera in a saddle-node bifurcation. The results help us understand the robustness of chimeras in networks of general oscillators to heterogeneity.

I. INTRODUCTION

Chimera states occur in networks of coupled oscillators and are characterised by coexisting groups of synchronised and asynchronous oscillators [1, 2]. They have been observed in one-dimensional [3, 4] and two-dimensional [5, 6] domains with nonlocal coupling, and also networks formed from two populations with strong coupling within a population and weaker coupling between them [7–9]. A variety of oscillator types have been considered, with the most common being a phase oscillator [10], but others include Stuart-Landau oscillators [11], van der Pol oscillators [4, 12], oscillators with inertia [13, 14] and neural models [15–17].

Many investigations of chimeras report only the results of numerically solving a finite number of ordinary differential equations (ODEs) which describe the networks' behaviour. Such simulations are for only a finite time, so the results seen may actually be part of a long transient [18]. With a finite network there is the issue of finite size effects, such as positive Lyapunov exponents which tend to zero as the network size is increased [2] or chimeras' finite lifetimes [19]. Perhaps most significantly, such simulations cannot detect unstable states so it is often not clear what happens to a stable chimera as a parameter is varied, other than it no longer existing.

Early results on the existence of chimeras used a self-consistency approach [10, 11, 20, 21] but this does not provide information on the stability of solutions. A great deal of progress has been made using the Ott/Antonsen ansatz [22, 23], since it gives evolution equations for quantities of interest, but its use is restricted to networks of phase oscillators coupled through sinusoidal functions of phase differences [2, 7, 24]. Laing [11] used self-consistency to investigate the existence of chimeras in networks of two populations of Stuart-Landau oscillators, each oscillator being described by a complex variable. This was later generalised [25] using techniques from [26] to determine the stability of these chimeras, and chimeras in networks of three more types of oscillators (Kuramoto with inertia, FitzHugh-Nagumo oscillators, delayed Stuart-Landau oscillators) were studied.

The approach in [25] was to recognise that the incoherent oscillators in one population lie on a curve $\mathcal{C}$ in the phase plane while those in the synchronous population can be described by a pair of real variables, since all of these oscillators are identical and undergo the same dynamics. In the limit of an infinite number of oscillators in each population the curve $\mathcal{C}$ is described by its shape (distance from the origin in polar coordinates) and the density of oscillators on it, and partial differential equations (PDEs) governing the evolution of these functions can be derived [26]. The full network is then described by a pair of PDEs and a pair of ODEs, coupled by an integral.

The analysis in [25] assumed *identical* oscillators, but we do not expect this to be the case in any experimental situation [27–29] and it is known that networks of identical oscillators may have qualitatively different dynamics from those of nonidentical oscillators [30]. In this paper we extend the results in [25] to the case of nonidentical oscillators. Specifically, we assume that for each oscillator, one parameter associated with its dynamics is randomly chosen from a uniform distribution. A uniform distribution is zero outside some range and this means that for a narrow distribution, the types of chimeras observed in [25] persist and can be described by a generalisation of the techniques developed in that paper.

---

* c.r.laing@massey.ac.nz

Various distributions of intrinsic frequencies in networks of all-to-all coupled oscillators have been considered, e.g. Lorentzian [22], bimodal [31], Gaussian [32, 33], beta [34] and uniform [35–39]. There are significant differences in the transition to synchrony as coupling strength is increased between distributions with compact support and those whose support is unbounded. In the former case one normally observes a first-order transition, whereas in the latter it is second-order. Also, for an infinite network full synchrony — in which all oscillators are phase locked — can only occur when the frequency distribution has compact support [40]. We observe and exploit this phenomenon to analyse the networks studied in this paper.

Previous relevant work includes [41], which considers a network formed from coupled ring subnetworks of logistic maps in which a number of parameters are randomly chosen from uniform distributions. The authors investigate the effects of varying the widths of these distributions on the number of subnetworks which fully synchronise.

We consider networks formed from two populations of oscillators. In Sec. II we consider Kuramoto-type phase oscillators and in Sec. III we revist the Stuart-Landau oscillators studied in [11]. Sec IV considers Kuramoto oscillators with inertia, also studied in [11]. We study van der Pol oscillators in Sec. V and conclude in Sec. VI.

II. KURAMOTO PHASE OSCILLATORS

We first consider two populations of phase oscillators coupled through a sinusoidal function of phase differences. Networks of this form have been studied previously [7–9, 42, 43]. We first consider heterogeneity in intrinsic frequencies, then in the strength of coupling between populations.

A. Distributed frequencies

Consider two populations of N phase oscillators each governed by

$$\frac{d\theta_j}{dt} = \omega_j + \frac{\mu}{N} \sum_{k=1}^{N} \sin\left(\theta_k - \theta_j - \alpha\right) + \frac{\nu}{N} \sum_{k=1}^{N} \sin\left(\theta_{N+k} - \theta_j - \alpha\right) \tag{1}$$

for $j = 1, 2 \ldots N$ and

$$\frac{d\theta_j}{dt} = \omega_j + \frac{\mu}{N} \sum_{k=1}^{N} \sin\left(\theta_{N+k} - \theta_j - \alpha\right) + \frac{\nu}{N} \sum_{k=1}^{N} \sin\left(\theta_k - \theta_j - \alpha\right) \tag{2}$$

for $j = N + 1, N + 2, \ldots 2N$. μ is the strength of coupling within a population and ν is the strength between populations. For identical ω_j this system reduces to the system studied in [7–9] while if they are chosen from a Lorentzian distribution it is the same as in [42]. Instead, here for each population the ω_j are randomly chosen from the uniform distribution $p(\omega)$ which is non-zero only on the interval B.

An example of a chimera state for (1)-(2) is shown in Fig. 1 where $p(\omega)$ is uniform on $[-\Delta\omega, \Delta\omega]$. We see that population 1 is incoherent, with no apparent dependence of θ_j on ω_j, whereas population 2 is synchronised (although not phase synchronised) with a clear dependence of θ_j on ω_j. The average frequencies of oscillators in the two populations are different, as required for a chimera state. [This state is close to the one which occurs for identical oscillators, so we also refer to it (and many states studied below) as a "chimera".] We now proceed to analyse this state, in terms of both existence and stability.

We assume that population 2 is locked, and write $\theta_{N+j} = \phi_j$ for $j = 1, 2, \ldots N$. Thus, using trigonometric identities, for population 2

$$\frac{d\phi_j}{dt} = \omega_{N+j} + \frac{\mu}{N} \sum_{k=1}^{N} \sin\left(\phi_k - \phi_j - \alpha\right) + \frac{\nu}{N} \sum_{k=1}^{N} \sin\left(\theta_k - \phi_j - \alpha\right)$$

$$= \omega_{N+j} + (\mu\hat{S} + \nu S)\cos\left(\phi_j + \alpha\right) - (\mu\hat{C} + \nu C)\sin\left(\phi_j + \alpha\right) \tag{3}$$

for $j = 1, 2, \ldots N$ where

$$\hat{S} \equiv \frac{1}{N} \sum_{k=1}^{N} \sin\phi_k; \qquad \hat{C} \equiv \frac{1}{N} \sum_{k=1}^{N} \cos\phi_k; \qquad S \equiv \frac{1}{N} \sum_{k=1}^{N} \sin\theta_k; \qquad C \equiv \frac{1}{N} \sum_{k=1}^{N} \cos\theta_k \tag{4}$$
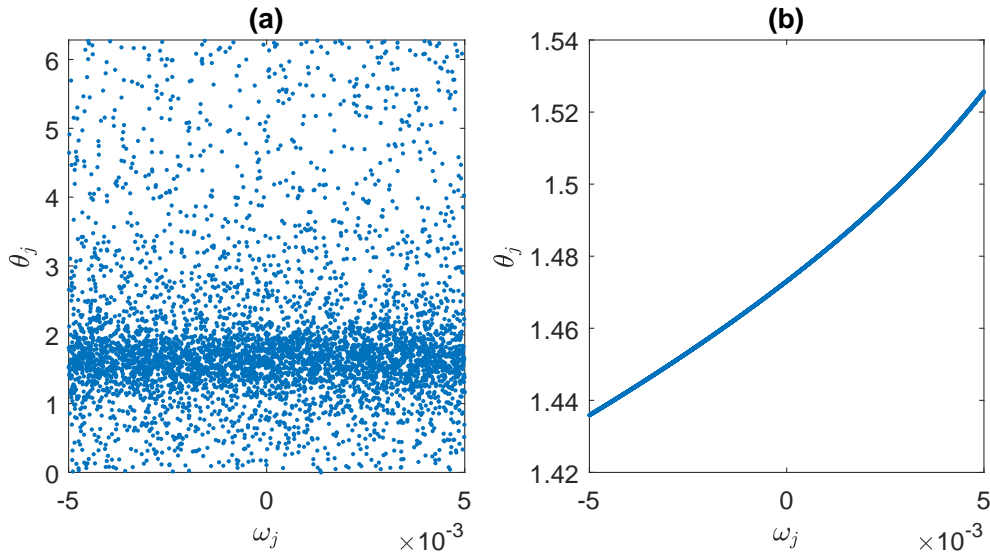
FIG. 1. A snapshot of a chimera state solution of (1)-(2). (a): population 1; (b): population 2. Note the different vertical axes. Parameters: $N = 5000, \mu = 0.6, \nu = 0.4, \alpha = \pi/2 - 0.08, \Delta\omega = 0.005$.

For population 1 we have

$$\frac{d\theta_j}{dt} = \omega_j + \text{Im}\left[e^{-i(\theta_j+\alpha)}\left(\frac{\mu}{N}\sum_{k=1}^{N}e^{i\theta_k} + \frac{\nu}{N}\sum_{k=1}^{N}e^{i\phi_k}\right)\right]$$

$$= \omega_j + \frac{1}{2i}\left[e^{-i(\theta_j+\alpha)}Z - e^{i(\theta_j+\alpha)}\bar{Z}\right] \tag{5}$$

where

$$Z \equiv \mu(C + iS) + \nu(\hat{C} + i\hat{S}) \tag{6}$$

and overline indicates complex conjugate. We now take the continuum limit $N \to \infty$. For population 2, instead of individual oscillators with phases ϕ_j and frequencies ω_j, ω is now a continuous parameter and we have the function $\phi(\omega, t)$, defined for $\omega \in B$. It satisfies the continuum version of (3):

$$\frac{\partial\phi(\omega, t)}{\partial t} = \omega + (\mu\hat{S} + \nu S)\cos(\phi + \alpha) - (\mu\hat{C} + \nu C)\sin(\phi + \alpha) \tag{7}$$

Fig. 1(b) can be regarded as showing $\phi(\omega, t)$ for the discrete values of ω used in the simulation, for a particular value of t.

In this limit we have

$$\hat{S} = \int_B \sin[\phi(\omega, t)]p(\omega)\ d\omega; \qquad \hat{C} = \int_B \cos[\phi(\omega, t)]p(\omega)\ d\omega \tag{8}$$

Population 1 is described by the probability density function $f(\theta, \omega, t)$ which satisfies the continuity equation

$$\frac{\partial f}{\partial t} + \frac{\partial}{\partial\theta}(fv) = 0 \tag{9}$$

where

$$v(\theta, \omega, t) = \omega + \frac{1}{2i}\left[e^{-i(\theta+\alpha)}Z - e^{i(\theta+\alpha)}\bar{Z}\right] \tag{10}$$

We can apply Ott/Antonsen ansatz [22, 23] and write

$$f(\theta, \omega, t) = \frac{p(\omega)}{2\pi}\left[1 + \sum_{n=1}^{\infty}a(\omega, t)^n e^{-in\theta} + \text{c.c.}\right] \tag{11}$$

where "c.c." is the complex conjugate of the previous term. Substituting this ansatz into the continuity equation above gives the evolution equation for $a(\omega, t)$ [22]:

$$\frac{\partial a(\omega, t)}{\partial t} = i\omega a + \frac{1}{2}\left(e^{-i\alpha}Z - e^{i\alpha}\bar{Z}a^2\right) \tag{12}$$

Lastly,

$$C + iS = \int_B \int_0^{2\pi} f(\theta, \omega, t)e^{i\theta} \, d\theta \, d\omega = \int_B a(\omega, t)p(\omega) \, d\omega \tag{13}$$

We move to a rotating coordinate frame rotating with angular speed Ω in which both a and ϕ are constant. Note that the phases of oscillators in population 1 are not constant in this frame, even though their density is. Thus we are interested in fixed points of

$$\frac{\partial a(\omega, t)}{\partial t} = i(\omega - \Omega)a + \frac{1}{2}\left(e^{-i\alpha}Z - e^{i\alpha}\bar{Z}a^2\right) \tag{14}$$

$$\frac{\partial \phi(\omega, t)}{\partial t} = \omega - \Omega + (\mu\hat{S} + \nu S)\cos(\phi + \alpha) - (\mu\hat{C} + \nu C)\sin(\phi + \alpha) \tag{15}$$

This is a pair of PDEs, one for the complex quantity a and the other for the angle ϕ, coupled through the integrals (8) and (13). The physical interpretation of ϕ is clear, and for fixed ω, the angular dependence of $f(\theta, \omega, t)$ is a Poisson kernel with centre given by the argument of $a(\omega, t)$ and its "sharpness" determined by the magnitude of $a(\omega, t)$ [24]. Eqns. (14)-(15) can be thought of as a generalisation of eqns. (11) in [7] to the case of nonidentical oscillators.

Due to the invariance under a global phase shift there is a continuum of fixed points of (14)-(15), each a shift of one another. Thus we append a "pinning" condition; in this case, $\hat{S} = 0$. This additional equation allows us to find all the unknowns, a, ϕ and Ω. We choose $p(\omega)$ to be uniform on $[-\Delta\omega, \Delta\omega]$ and use Gauss-Legendre quadrature with 50 points to approximate the integrals. Thus the domain $[-\Delta\omega, \Delta\omega]$ is discretised using the points $\omega_i = \Delta\omega x_i$ for $i = 1, 2, \ldots 50$ where the x_i are the roots of $P_{50}(x)$, the Legendre polynomial of order 50. The integrals over ω in (8) and (13) are thus approximated by weighted sums.

1. Results

The most obvious question is: what is the influence of having distributed values of ω on the existence and stability of chimeras? Using pseudo-arclength continuation [44, 45] and varying $\Delta\omega$ we obtain Fig. 2. The stable chimera that exists for identical oscillators is destroyed in a saddle-node bifurcation as $\Delta\omega$ is increased, i.e. the oscillators are made more heterogeneous. This is in contrast to the situation when the ω_j are chosen from a Lorentzian distribution, where increasing the level of heterogeneity causes the distribution of phases in the chimera to become more peaked and the distribution in the synchronous group to be come less peaked until both states meet in a pitchfork bifurcation and merge to form a state in which the two populations cannot be distinguished [42].

The ϕ component of the eigenvector corresponding to the zero eigenvalue at the saddle-node bifurcation is shown in Fig. 3 and it is clear that this is localised at the highest ω_i, i.e. it is the oscillator with the largest intrinsic frequency which "unlocks" first as $\Delta\omega$ is increased, leading to "phase walkthrough" [46].

A typical set of eigenvalues of the linearisation about a fixed point of (14)-(15) is shown in Fig. 4. Recall that we have discretised ω with 50 points. We see 49 points on the negative real axis, each corresponding to a perturbation localised at one or two neighbouring ϕ values. There are also 49 complex conjugate pairs with zero real part, each corresponding to a perturbation localised at one or two neighbouring a values. These 147 eigenvalues are associated with discretising the continuous parameter ω, and are presumably discretisations of the continuous spectrum associated with fixed points of (14)-(15). There is also a complex conjugate pair with negative real part which, upon varying the relative sizes of μ and ν, could cross the imaginary axis resulting in a Hopf bifurcation [7], and the single zero eigenvalue corresponding to the invariance of the system under a global phase shift. As $\Delta\omega \to 0$, the 49 negative real eigenvalues collapse to a single negative real value with multiplicity 49, and the 49 complex conjugate pairs on the imaginary axis collapse to a single complex conjugate pair on the imaginary axis, again with multiplicity 49.

Thus the term "stable" when referring to solutions in Fig. 2 actually means "neutrally stable" or "not unstable". Indeed, when numerically integrating (14)-(15) the system may not approach a fixed point even in a rotating coordinate frame, but the fixed point can still be found using Newton's method. A similar phenomenon was observed in [8], and this is reflective of the fact that when (14) is discretised in ω, the equation for each ω describes the dynamics of a network of identical oscillators, whose dynamics is more fully described by the equations derived using the
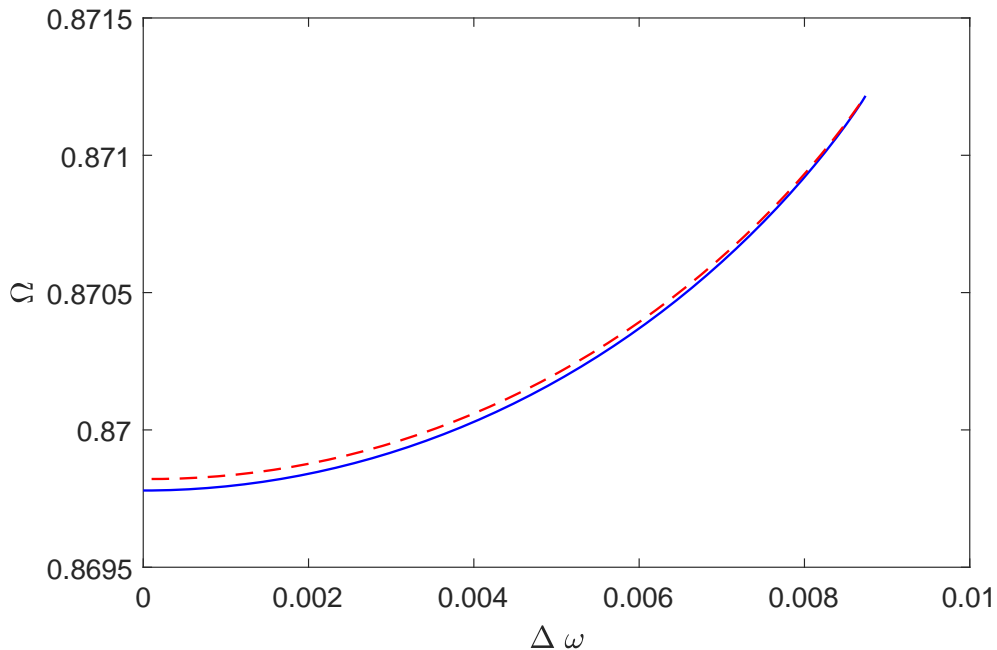
FIG. 2. Ω for fixed points of (14)-(15) describing chimera states. Solid: "stable". Dashed: unstable. Parameters: $\mu = 0.6, \nu = 0.4, \alpha = \pi/2 - 0.08$.

Watanabe/Strogatz ansatz [30, 47]. (The Ott/Antonsen ansatz is a special case of the Watanabe/Strogatz ansatz, corresponding to an infinite number of identical oscillators, with a uniform distribution of certain constants [8].)

Note that chimeras have been seen in similar networks with uniformly distributed frequencies [48], but in the models studied there the coupling strength within and between populations was a function of the level of synchrony within the populations, not a constant, as here.

B. Heterogeneous between-population coupling strengths

Now, as another example, consider having heterogeneous ν values, i.e. replace (1) with

$$\frac{d\theta_j}{dt} = \omega + \frac{\mu}{N} \sum_{k=1}^{N} \sin\left(\theta_k - \theta_j - \alpha\right) + \frac{\nu_j}{N} \sum_{k=1}^{N} \sin\left(\theta_{N+k} - \theta_j - \alpha\right) \tag{16}$$

and replace (2) in an equivalent way. Take the ν_j from $p(\nu)$, a uniform distribution on $[\nu_0 - \Delta\nu, \nu_0 + \Delta\nu]$. In a similar way to above we derive the evolution equations

$$\frac{\partial a(\nu, t)}{\partial t} = -i\Omega a + \frac{1}{2}\left(e^{-i\alpha}Z - e^{i\alpha}\bar{Z}a^2\right) \tag{17}$$

$$\frac{\partial \phi(\nu, t)}{\partial t} = -\Omega + (\mu\hat{S} + \nu S)\cos\left(\phi + \alpha\right) - (\mu\hat{C} + \nu C)\sin\left(\phi + \alpha\right) \tag{18}$$

where now

$$\hat{S} = \int_{B} \sin\left[\phi(\nu, t)\right]p(\nu)\ d\nu; \qquad \hat{C} = \int_{B} \cos\left[\phi(\nu, t)\right]p(\nu)\ d\nu \tag{19}$$

and

$$C + iS = \int_{B} a(\nu, t)p(\nu)\ d\nu, \tag{20}$$

B is the interval $[\nu_0 - \Delta\nu, \nu_0 + \Delta\nu]$, and without loss of generality we have set $\omega = 0$. Note that Z, defined through (6), is not longer a scalar, but a function of the continuous parameter ν. Following fixed points of (17)-(18) as $\Delta\nu$ is
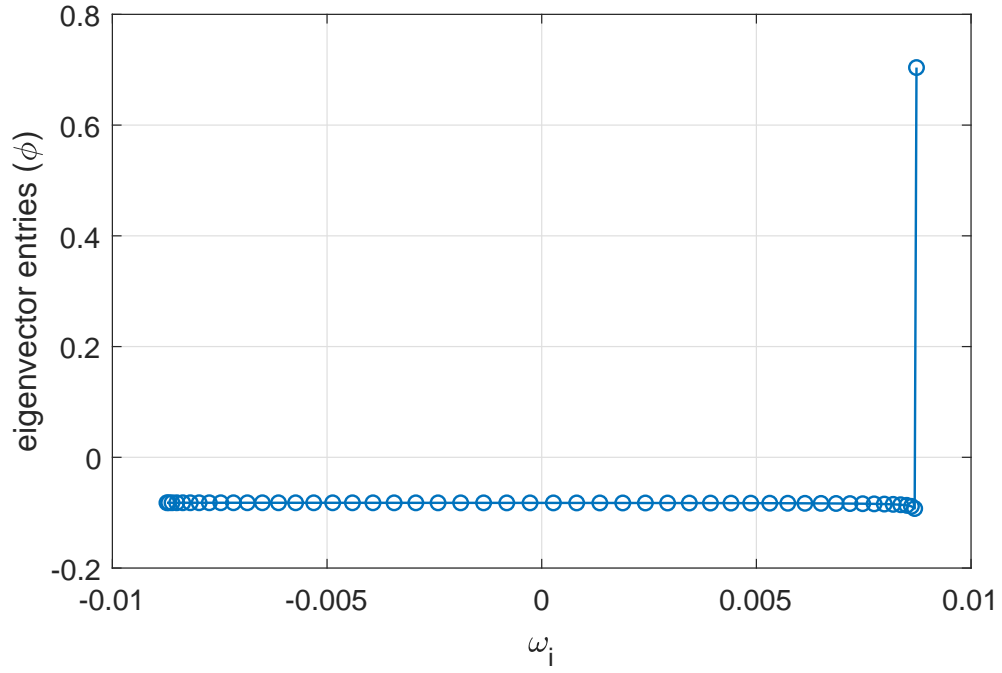
FIG. 3. Eigenvector localisation. ϕ component of the eigenvector corresponding to the zero eigenvalue at the saddle-node bifurcation shown in Fig. 2. Parameters: $\mu = 0.6, \nu = 0.4, \alpha = \pi/2 - 0.08, \Delta\omega = 0.0087392$.
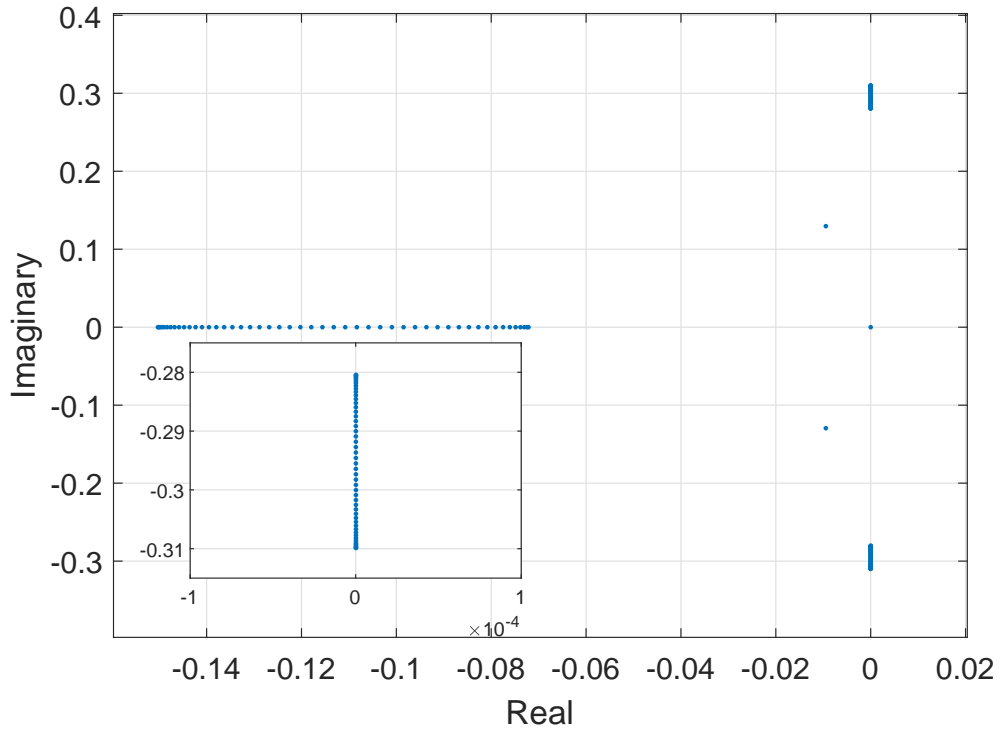

FIG. 4. Eigenvalues of the linearisation about a fixed point of (14)-(15). The inset shows a zoom of the main figure. Parameters: $\mu = 0.6, \nu = 0.4, \alpha = \pi/2 - 0.08, \Delta\omega = 0.005$.
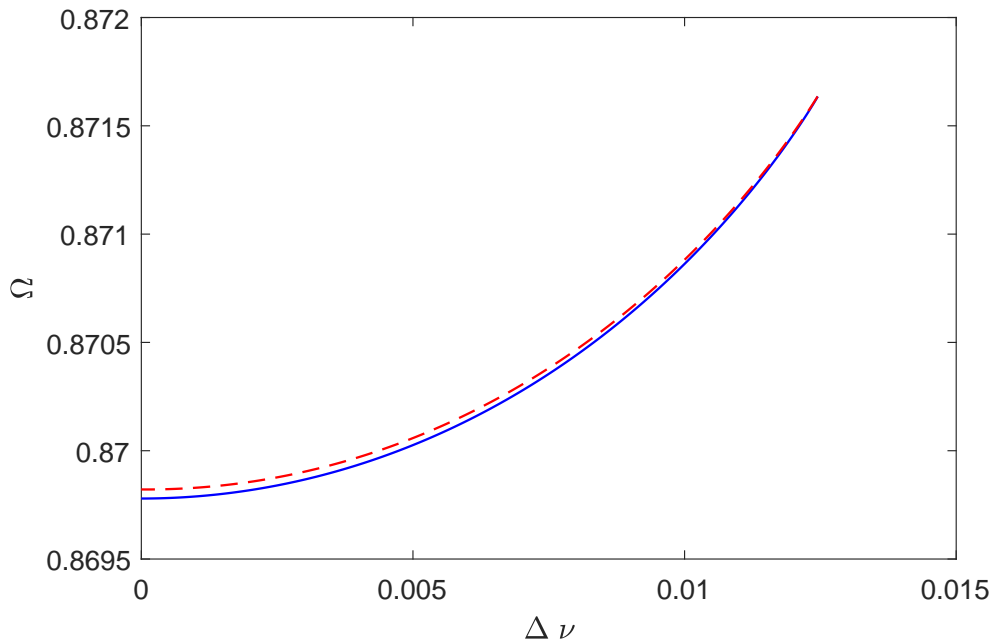
FIG. 5. Ω for fixed points of (17)-(18) describing chimera states. Solid: "stable". Dashed: unstable. Parameters: $\mu = 0.6, \nu_0 = 0.4, \alpha = \pi/2 - 0.08$.

increased we obtain Fig. 5, which is very similar to Fig. 2. The eigenvalues of the linearisation about a "stable" state in Fig. 5 are similar to those shown in Fig. 4, for similar reasons as discussed above.

We could perform similar analyses for the other two parameters, α and μ, but now move on to oscillators described by two variables.

III.   STUART-LANDAU OSCILLATORS

We now consider the chimera state found in [11] in a network of two populations of Stuart-Landau oscillators, each oscillator being described by a complex variable.

A.   Heterogeneous frequencies

The equations governing the dynamics are

$$\frac{dX_j}{dt} = i\omega_j X_j + \epsilon^{-1}\{1 - (1 + \delta\epsilon i)|X_j|^2\}X_j + e^{-i\alpha}\left(\frac{\mu}{N}\sum_{k=1}^{N} X_k + \frac{\nu}{N}\sum_{k=1}^{N} X_{N+k}\right) \tag{21}$$

for $j = 1, \ldots N$ and

$$\frac{dX_j}{dt} = i\omega_j X_j + \epsilon^{-1}\{1 - (1 + \delta\epsilon i)|X_j|^2\}X_j + e^{-i\alpha}\left(\frac{\mu}{N}\sum_{k=1}^{N} X_{N+k} + \frac{\nu}{N}\sum_{k=1}^{N} X_k\right) \tag{22}$$

for $j = N + 1, \ldots 2N$, where each $X_j \in \mathbb{C}$ and $\epsilon, \delta, \alpha, \mu$ and ν are all real parameters. As before, μ is the strength of coupling within a population and ν is the strength between populations. The ω_j are randomly chosen from the uniform distribution on $[-\Delta\omega, \Delta\omega]$.

An example of a stable chimera for (21)-(22) is shown in Fig. 6, with oscillators coloured by their ω_j value. (A similar figure appears in [25].) We see that population 2 is synchronised and the oscillators lie on an open curve, with their position on the curve determined by their heterogeneous parameter ω_j. Population 1 is incoherent, and there seems to be no correlation between an oscillator's position and its ω_j value. The oscillators in population 1 seem to
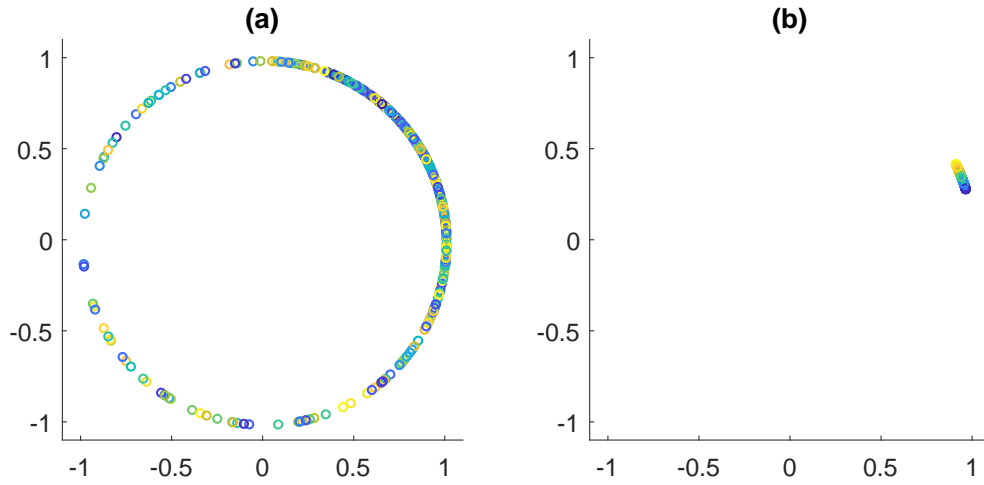
FIG. 6. A snapshot of a chimera state solution of (21)-(22), showing the X_j in the complex plane. The points are coloured by their ω_j value. (a): population 1; (b): population 2. Parameters: $N = 500, \epsilon = 0.05, \delta = -0.01, \mu = 0.6, \nu = 0.4, \alpha = \pi/2 - 0.08, \Delta\omega = 0.01$.

all lie on a single closed curve, but we will see below that oscillators with different values of ω_j actually lie on slightly different curves, and move along these curves with slightly different average frequencies.

To analyse a chimera state let $X_{N+j} = Y_j$ for $j \in \{1, \dots N\}$ where the Y_j rotate around the origin at the same speed, i.e. population two is synchronised. Letting

$$\widehat{X} = \frac{1}{N}\sum_{k=1}^{N} X_k \qquad \text{and} \qquad \widehat{Y} = \frac{1}{N}\sum_{k=1}^{N} Y_k \tag{23}$$

we have

$$\frac{dY_j}{dt} = i\omega_{N+j}Y_j + \epsilon^{-1}\{1 - (1+\delta\epsilon i)|Y_j|^2\}Y_j + e^{-i\alpha}\left(\mu\widehat{Y} + \nu\widehat{X}\right) \tag{24}$$

for $j = 1, \dots N$ and each oscillator in population one satisfies

$$\frac{dX_j}{dt} = i\omega_j X_j + \epsilon^{-1}\{1 - (1+\delta\epsilon i)|X_j|^2\}X_j + e^{-i\alpha}\left(\mu\widehat{X} + \nu\widehat{Y}\right), \tag{25}$$

for $j = 1, \dots N$. Converting to polar coordinates for population 1 by writing $X_j = r_j e^{i\phi_j}$ we have

$$\frac{dr_j}{dt} = \epsilon^{-1}(1 - r_j^2)r_j + \text{Re}\left[e^{-i(\alpha+\phi_j)}\left(\mu\widehat{X} + \nu\widehat{Y}\right)\right] \equiv F(r_j, \phi_j, \widehat{X}, \widehat{Y}) \tag{26}$$

$$\frac{d\phi_j}{dt} = \omega_j - \delta r_j^2 + \frac{1}{r_j}\text{Im}\left[e^{-i(\alpha+\phi_j)}\left(\mu\widehat{X} + \nu\widehat{Y}\right)\right] \equiv G(r_j, \phi_j, \widehat{X}, \widehat{Y}, \omega_j) \tag{27}$$

We now take the continuum limit of $N \to \infty$. Eqn (24) is replaced by

$$\frac{\partial Y}{\partial t}(\omega, t) = i\omega Y + \epsilon^{-1}\{1 - (1+\delta\epsilon i)|Y|^2\}Y + e^{-i\alpha}\left(\mu\widehat{Y} + \nu\widehat{X}\right) \tag{28}$$

Generalising the theory from [25, 26], we assume that oscillators with a particular value of ω lie on a curve $\mathcal{C}(\omega)$ in the complex plane parametrised by the angle from the positive real axis, ϕ. The distance from the origin to $\mathcal{C}(\omega)$ at angle ϕ is $R(\phi, t; \omega)$ and the density of oscillators at this point is $P(\phi, t; \omega)$. The evolution of the functions R and P is given by

$$\frac{\partial R}{\partial t}(\phi, t; \omega) = F(R, \phi, \widehat{X}, \widehat{Y}) - G(R, \phi, \widehat{X}, \widehat{Y}, \omega)\frac{\partial R}{\partial \phi} \tag{29}$$

$$\frac{\partial P}{\partial t}(\phi, t; \omega) = -\frac{\partial}{\partial \phi}\left[P(\phi, t; \omega)G(R, \phi, \widehat{X}, \widehat{Y}, \omega)\right] + D\frac{\partial^2}{\partial \phi^2}P(\phi, t; \omega) \tag{30}$$
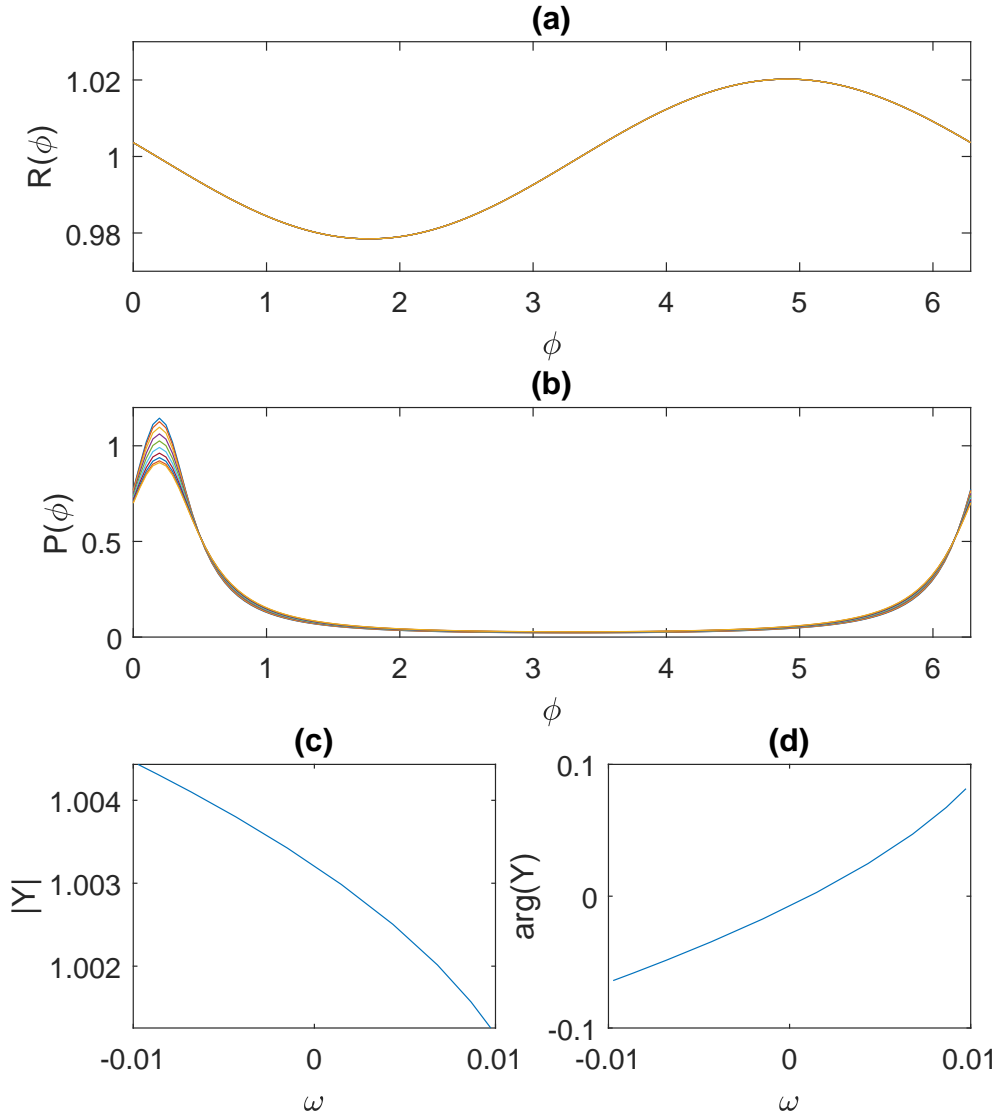
FIG. 7. Snapshot of a solution of (29)-(32) for which $\widehat{Y}$ is real. This solution is stationary in a coordinate frame rotating at $\Omega = 0.86678$. (a): $R(\phi)$ for the 10 different values of ω_i, (b): $P(\phi)$ for the 10 different values of ω_i. (c) and (d): modulus and argument of Y, respectively, as functions of ω. Parameters: $\epsilon = 0.05, \delta = -0.01, \mu = 0.6, \nu = 0.4, \alpha = \pi/2 - 0.08, D = 10^{-8}, \Delta\omega = 0.01$.

where for numerical stability reasons we have added a small amount of diffusion, of strength D, to (30) (as did [26]). In the continuum limit we have

$$\widehat{X} = \int_B p(\omega) \int_0^{2\pi} P(\phi, t; \omega) R(\phi, t; \omega) e^{i\phi} d\phi \ d\omega \tag{31}$$

and

$$\widehat{Y} = \int_B Y(\omega, t) p(\omega) \ d\omega \tag{32}$$

where B is the support of the uniform density $p(\omega)$. The equations (28)-(32) form a set of PDEs, coupled through integrals. Note that (21)-(22) are invariant under the global phase shift $X_j \mapsto X_j e^{i\gamma}$ for any constant γ and thus we can move to a rotating coordinate frame in which $Y(\omega, t)$ is constant. Moving to a coordinate frame rotating with speed Ω has the effect of replacing the ω_j in (27) by $\omega_j - \Omega$ and the ω in (28) by $\omega - \Omega$.

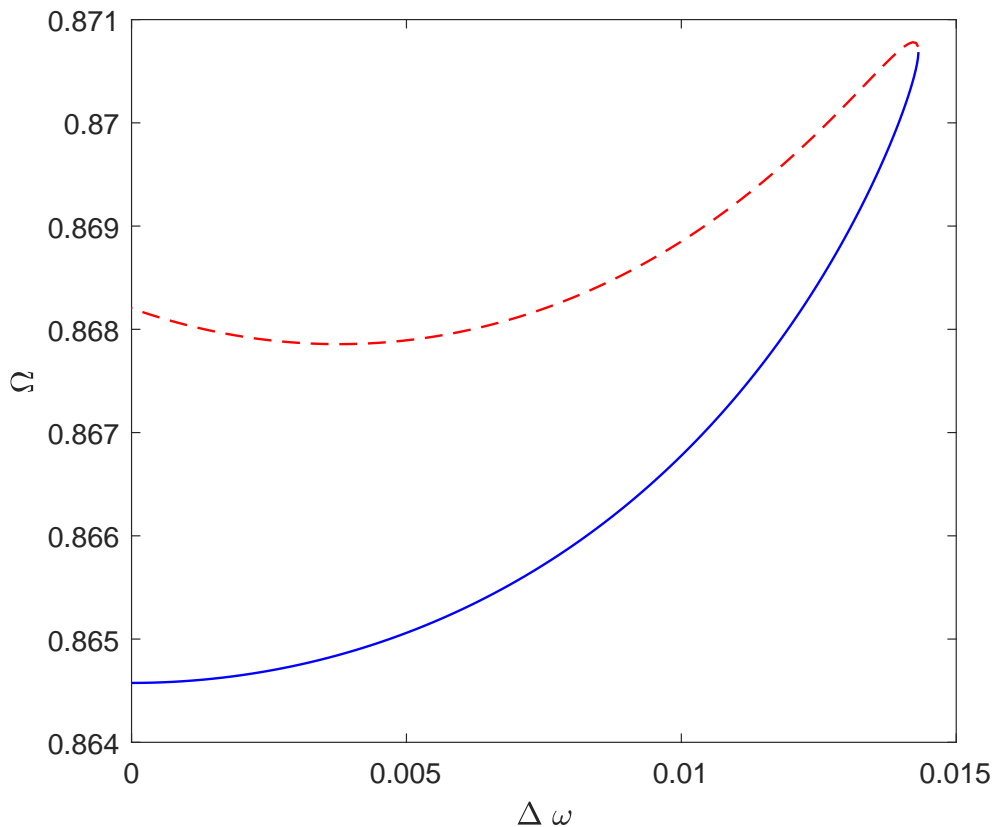FIG. 8. Ω as a function of $\Delta\omega$ for fixed points (in a rotating coordinate frame) of (28)-(32) describing a chimera. Solid: stable; dashed: unstable. Parameters: $\epsilon = 0.05, \delta = -0.01, \mu = 0.6, \nu = 0.4, \alpha = \pi/2 - 0.08, D = 10^{-8}$.

1. Results

We numerically integrate (28)-(32) in time to find a stable solution. An example is shown in Fig. 7. We see that $R(\phi)$ depends very weakly on ω (the distance between curves in panel (a) is $\sim 10^{-5}$) whereas $P(\phi)$ depends more strongly on ω. We discretised ϕ using 128 equally-spaced points and implemented derivatives with respect to ϕ spectrally [49]. $p(\omega)$ is uniform on $[-\Delta\omega, \Delta\omega]$ and we implement the integrals over ω in (31)-(32) using Gauss-Legendre quadrature with 10 points, so the discrete values of ω used are $\omega_i = \Delta\omega x_i$ for $i = 1, 2, \ldots 10$ where the x_i are the roots of $P_{10}(x)$, the Legendre polynomial of order 10. For each ω_i we enforce conservation of probability by setting P at one angular grid point equal to $1/(\Delta\phi)$ minus the sum of the values at all other grid points, where $\Delta\phi = 2\pi/128$, the ϕ grid spacing [50].

Moving to a rotating coordinate frame and following a steady state of (28)-(32) in that frame as $\Delta\omega$ is increased we obtain Fig. 8. As in Sec. II A 1 we see that the stable solution is destroyed in a saddle-node bifurcation. The eigenvalues of the linearisation about a stable state are similar to those in Fig. 3 of [25] and Fig. 5 in [26], i.e. they form two clusters (not shown). Those in the cluster with large negative real part are associated with perturbations in the R component of the dynamics while those in the other cluster which are almost marginally stable are associated with perturbations in the P component.

We know from [25] that if $\Delta\omega = 0$, increasing ϵ will also destroy the chimera in a saddle-node bifurcation. Following this bifurcation and the one in Fig. 8 we obtain Fig. 9, where the former bifurcation is shown in blue and the latter in red. Interestingly, they are not part of the same curve. Both curves of saddle-node bifurcations have Takens-Bogdanov points on them, at which point the linearisation of the dynamics around the fixed point has a double zero eigenvalue [51, 52]. At both of these points a curve of Hopf bifurcations is created, as seen in Fig. 9. We expect other global bifurcations in the vicinity of these points, but finding them numerically is difficult.
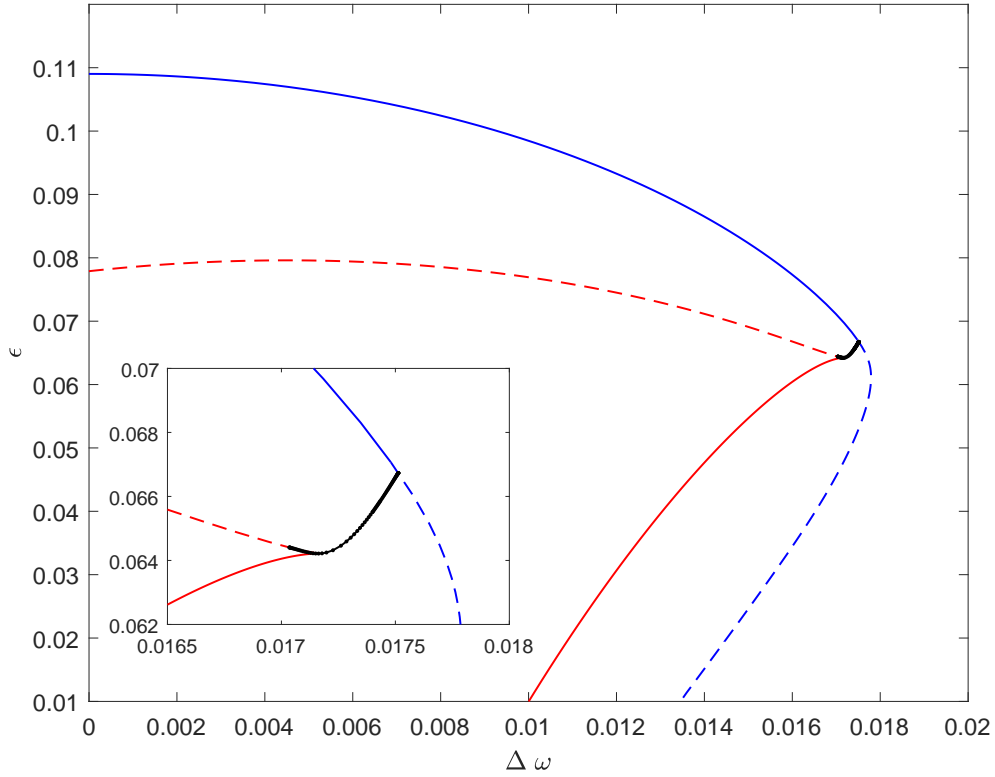
FIG. 9. Saddle-node bifurcation curves (red and blue) and Hopf bifurcation curve (black) for fixed points of chimera solutions of (28)-(32). The inset shows a zoom of the Hopf bifurcation curve. The chimera is stable to the left of and below the solid curves, and above the Hopf bifurcation curve. Parameters: $\delta = -0.01, \mu = 0.6, \nu = 0.4, \alpha = \pi/2 - 0.08, D = 10^{-8}$.

B. Heterogeneous between-population coupling strengths

Now consider heterogeneity in ν. We replace (21) by

$$\frac{dX_j}{dt} = i\omega X_j + \epsilon^{-1}\{1 - (1 + \delta\epsilon i)|X_j|^2\}X_j + e^{-i\alpha}\left(\frac{\mu}{N}\sum_{k=1}^{N} X_k + \frac{\nu_j}{N}\sum_{k=1}^{N} X_{N+k}\right) \tag{33}$$

for $j = 1, 2, \ldots N$ and similarly for population 2, and choose the ν_j from a uniform distribution on $[\nu_0 - \Delta\nu, \nu_0 + \Delta\nu]$. Choosing $\mu = 0.625$ and $\nu_0 = 0.375$ (and $\delta = -0.01, \alpha = \pi/2 - 0.08$) we know from [25] that if $\Delta\nu = 0$, increasing ϵ results in the stable chimera undergoing a supercritical Hopf bifurcation. Increasing $\Delta\nu$ for $\epsilon = 0.03$ we find a saddle-node bifurcation at $\Delta\nu \approx 0.156$ and following these two bifurcations we obtain Fig. 10.

The curves meet in a saddle-node/Hopf bifurcation, where the linearisation about the fixed point has both a zero eigenvalue and a complex conjugate pair of purely imaginary eigenvalues [51, 52]. Stationary chimeras of the form we are considering (where Y is constant in a uniformly-rotating coordinate frame) exist only to the left of the saddle-node bifurcation curve. Stable stationary states of this form only exist in the region bounded by the axes and the solid curves in Fig. 10. They become unstable through a supercritical Hopf bifurcation as ϵ is increased, leading to stable periodic chimeras.

To better understand Fig. 10, for $\epsilon = 0.05$, as $\Delta\nu$ is decreased and the dashed saddle-node curve is crossed, a pair of fixed points is created, one with three unstable eigenvalues and one with two. As $\Delta\nu$ is further decreased the fixed point with three unstable eigenvalues undergoes a Hopf bifurcation, gaining two stable directions. So between the solid and dashed Hopf bifurcation curves one fixed point has one unstable eigenvalue and the other has two. As ϵ is then decreased the fixed point with two unstable eigenvalues undergoes a Hopf bifurcation, becoming stable. If $\Delta\nu$ is then increased, this stable fixed point is destroyed in a saddle-node bifurcation with the fixed point having one unstable eigenvalue. We expect there to be other curves of global bifurcations in a neighbourhood of the saddle-node/Hopf bifurcation, but finding them is numerically difficult.
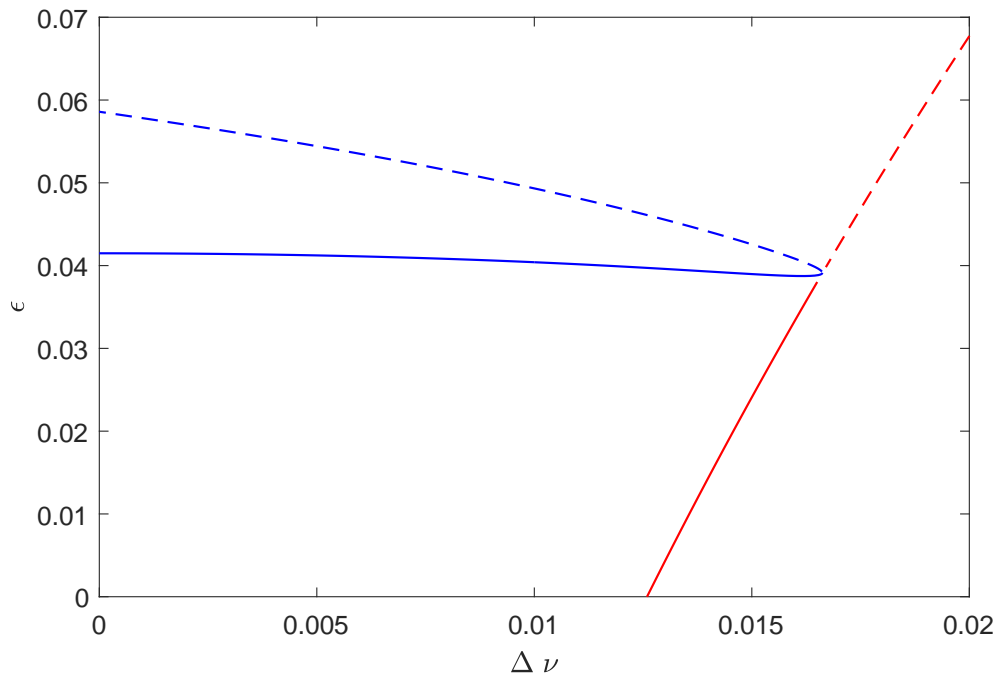
FIG. 10. Saddle-node bifurcation (red) and Hopf bifurcation (blue) for fixed points of (28)-(32). There is a stable stationary chimera in the region bounded by the axes and the solid curves. There is a stable periodic chimera above the lower (solid blue) Hopf bifurcation curve. Parameters: $\delta = -0.01, \mu = 0.625, \nu_0 = 0.375, \alpha = \pi - 0.08, D = 10^{-8}, \omega = 0$.

IV. KURAMOTO WITH INERTIA

We now consider a network formed from two populations of N Kuramoto oscillators with inertia, where we have heterogeneity in frequencies. The system is described by

$$m\frac{d^2\theta_i^{(1)}}{dt^2} + \frac{d\theta_i^{(1)}}{dt} = \omega_i^{(1)} + \frac{\mu}{N}\sum_{j=1}^{N}\sin\left(\theta_j^{(1)} - \theta_i^{(1)} - \alpha\right) + \frac{\nu}{N}\sum_{j=1}^{N}\sin\left(\theta_j^{(2)} - \theta_i^{(1)} - \alpha\right) \quad (34)$$

$$m\frac{d^2\theta_i^{(2)}}{dt^2} + \frac{d\theta_i^{(2)}}{dt} = \omega_i^{(2)} + \frac{\mu}{N}\sum_{j=1}^{N}\sin\left(\theta_j^{(2)} - \theta_i^{(2)} - \alpha\right) + \frac{\nu}{N}\sum_{j=1}^{N}\sin\left(\theta_j^{(1)} - \theta_i^{(2)} - \alpha\right) \quad (35)$$

where m is "mass", μ, ν and α are parameters, and the superscript labels the population. When $m = 0$ and the ω_i are all equal this reverts to a previously studied case [7, 8]. With $m = 0$ and ω_i chosen from a uniform distribution it reverts to that studied in Sec. II A, while for $m \neq 0$ and the ω_j being chosen from a Lorentzian it is that studied in [13]. These authors found apparently stable chimeras for finite networks of oscillators. With $m \neq 0$ and identical ω_j it is the same as studied in [14].

In [25] it was found that with $m \neq 0$ and identical ω_i the apparently stable chimera solution found by simulating (34)-(35) was actually (weakly) unstable when the continuum equations were studied, with the real part of the rightmost eigenvalues determining its stability increasing with m. So it is of interest to investigate the effects of heterogeneity in the ω_j on such a state: does it stabilise this state?
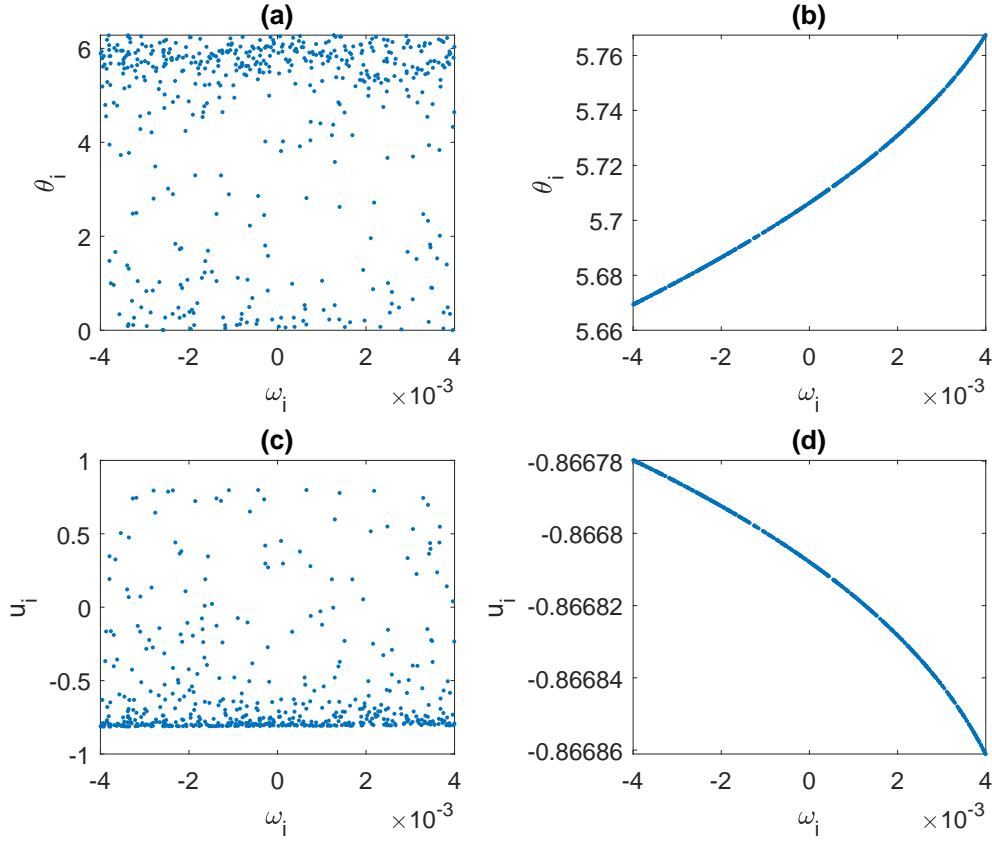
FIG. 11. A snapshot of a chimera state for (36)-(39). Population 1 is on the left and population 2 is on the right. Note the different vertical scales. Parameters: $N = 500, m = 0.1, \mu = 0.6, \nu = 0.4, \alpha = \pi/2 - 0.05, \Delta\omega = 0.004$.

We rewrite the equations as

$$\frac{d\theta_i^{(1)}}{dt} = u_i^{(1)} \tag{36}$$

$$\frac{du_i^{(1)}}{dt} = \left[\omega_i^{(1)} - u_i^{(1)} + \frac{\mu}{N} \sum_{j=1}^{N} \sin\left(\theta_j^{(1)} - \theta_i^{(1)} - \alpha\right) + \frac{\nu}{N} \sum_{j=1}^{N} \sin\left(\theta_j^{(2)} - \theta_i^{(1)} - \alpha\right) \right] / m \tag{37}$$

$$\frac{d\theta_i^{(2)}}{dt} = u_i^{(2)} \tag{38}$$

$$\frac{du_i^{(2)}}{dt} = \left[\omega_i^{(2)} - u_i^{(2)} + \frac{\mu}{N} \sum_{j=1}^{N} \sin\left(\theta_j^{(2)} - \theta_i^{(2)} - \alpha\right) + \frac{\nu}{N} \sum_{j=1}^{N} \sin\left(\theta_j^{(1)} - \theta_i^{(2)} - \alpha\right) \right] / m \tag{39}$$

A snapshot of a stable chimera state for (36)-(39) is shown in Fig. 11, where for both populations the ω_i are taken from a uniform distribution on $[-\Delta\omega, \Delta\omega]$. We see that population 1 is incoherent while population 2 is synchronised with both θ_i and u_i being smooth functions of ω_i.

To analyse this state let us assume that population two is synchronised, with $\theta_k^{(2)} = \Theta_k$ and $u_k^{(2)} = U_k$ for $k = 1, 2 \ldots N$. We drop the superscripts for variables in population 1. Oscillators in population 2 satisfy

$$\frac{d\Theta_k}{dt} = U_k \tag{40}$$

$$\frac{dU_k}{dt} = \left[\omega_k^{(2)} - U_k + \mu \text{Im} \left\{ e^{-i(\Theta_k + \alpha)} Y \right\} + \nu \text{Im} \left\{ e^{-i(\Theta_k + \alpha)} X \right\} \right] / m \tag{41}$$

where

$$X \equiv \frac{1}{N} \sum_{j=1}^{N} e^{i\theta_j} \in \mathbb{C}, \qquad Y = \frac{1}{N} \sum_{j=1}^{N} e^{i\Theta_j} \in \mathbb{C} \tag{42}$$

Oscillators in population 1 satisfy

$$\frac{d\theta_k}{dt} = u_k \tag{43}$$

$$\frac{du_k}{dt} = \left[\omega_k^{(1)} - u_k + \mu \text{Im} \left\{ e^{-i(\theta_k + \alpha)} X \right\} + \nu \text{Im} \left\{ e^{-i(\theta_k + \alpha)} Y \right\} \right] / m \tag{44}$$

for $k = 1, \ldots N$. We put these equations in "polar" form by defining $r_k = 2 + u_k$ (adding 2 bounds the r_k away from zero) and thus we have

$$\frac{dr_k}{dt} = \left[\omega_k^{(1)} - (r_k - 2) + \mu \text{Im} \left\{ e^{-i(\theta_k + \alpha)} X \right\} + \nu \text{Im} \left\{ e^{-i(\theta_k + \alpha)} Y \right\} \right] / m$$

$$\equiv F(r_k, \theta_k, X, Y, \omega_k^{(1)}) \tag{45}$$

$$\frac{d\theta_k}{dt} = r_k - 2 \tag{46}$$

For the chimera state of interest, Θ_k and U_k are stationary in a coordinate frame rotating at speed Ω. Moving to this coordinate frame has the effect of replacing (40) by

$$\frac{d\Theta_k}{dt} = U_k + \Omega \tag{47}$$

and (46) by

$$\frac{d\theta_k}{dt} = r_k - 2 + \Omega \equiv G(r_k, \theta_k, X, Y) \tag{48}$$

Taking the limit $N \to \infty$ we consider the dynamical system

$$\frac{\partial R}{\partial t}(\theta, t; \omega) = F(R, \theta, X, Y, \omega) - G(R, \theta, X, Y) \frac{\partial R}{\partial \theta} \tag{49}$$

$$\frac{\partial P}{\partial t}(\theta, t; \omega) = -\frac{\partial}{\partial \theta} \left[P(\theta, t; \omega) G(R, \theta, X, Y) \right] + D \frac{\partial^2}{\partial \theta^2} P(\theta, t; \omega) \tag{50}$$

along with

$$\frac{\partial \Theta}{\partial t}(\omega, t) = U + \Omega \tag{51}$$

and

$$\frac{\partial U}{\partial t}(\omega, t) = \left[\omega - U + \mu \text{Im} \left\{ e^{-i(\Theta + \alpha)} Y \right\} + \nu \text{Im} \left\{ e^{-i(\Theta + \alpha)} X \right\} \right] / m \tag{52}$$

where

$$X(t) = \int_B p(\omega) \int_0^{2\pi} P(\theta, t; \omega) R(\theta, t; \omega) e^{i\theta} d\theta \, d\omega \tag{53}$$

and

$$Y(t) = \int_B e^{i\Theta(\omega, t)} p(\omega) d\omega \tag{54}$$

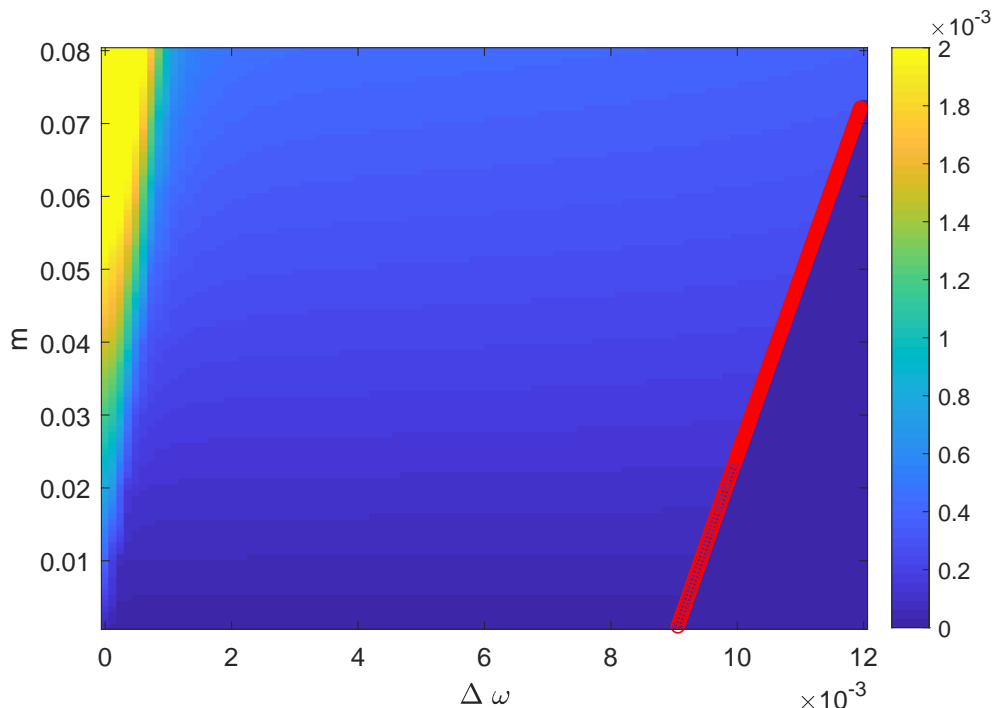and B is the interval $[-\Delta\omega, \Delta\omega]$.

FIG. 12. The red circles show a saddle-node bifurcation, to the right of which solutions in which all oscillators in population 2 for (49)-(54) are locked do not exist. The colour is the real part of the rightmost eigenvalues determining the stability of the chimera (truncated above 2×10^{-3}), which is always positive. Parameters: $\mu = 0.6, \nu = 0.4, \alpha = \pi/2 - 0.05, D = 10^{-13}$. θ is discretised with 128 points and ω with 10.

A. Results

For small values of $m, \Delta\omega$ and D, stable chimera solutions of (49)-(54) can be found, but as in [25], decreasing D to 10^{-13} we find that they are actually weakly unstable. Following them as $\Delta\omega$ is increased we find that they are destroyed in a saddle-node bifurcation, as shown in Fig. 12. To the left of this curve these solutions are always unstable, although (as in [25]) they become less unstable as m is decreased. Although making the oscillators heterogeneous in this way does not fully stabilise the chimera, it does make then less unstable, as can be seen by varying $\Delta\omega$ for a fixed value of m in Fig. 12. In summary, as in [25], for the parameters chosen, stable chimeras do not exist for infinite networks described by (49)-(54) even with ω values chosen from a uniform distribution.

V. VAN DER POL OSCILLATORS

We lastly consider two populations of van der Pol oscillators, governed by

$$\frac{dx_i}{dt} = y_i \tag{55}$$

$$\frac{dy_i}{dt} = \epsilon(1 - x_i^2)y_i - x_i + \mu[b_i(\bar{X}_1 - x_i) + c(\bar{Y}_1 - y_i)] + \nu[b_i(\bar{X}_2 - x_i) + c(\bar{Y}_2 - y_i)] \tag{56}$$

for $i = 1, 2 \ldots N$ and

$$\frac{dx_i}{dt} = y_i \tag{57}$$

$$\frac{dy_i}{dt} = \epsilon(1 - x_i^2)y_i - x_i + \mu[b_i(\bar{X}_2 - x_i) + c(\bar{Y}_2 - y_i)] + \nu[b_i(\bar{X}_1 - x_i) + c(\bar{Y}_1 - y_i)] \tag{58}$$
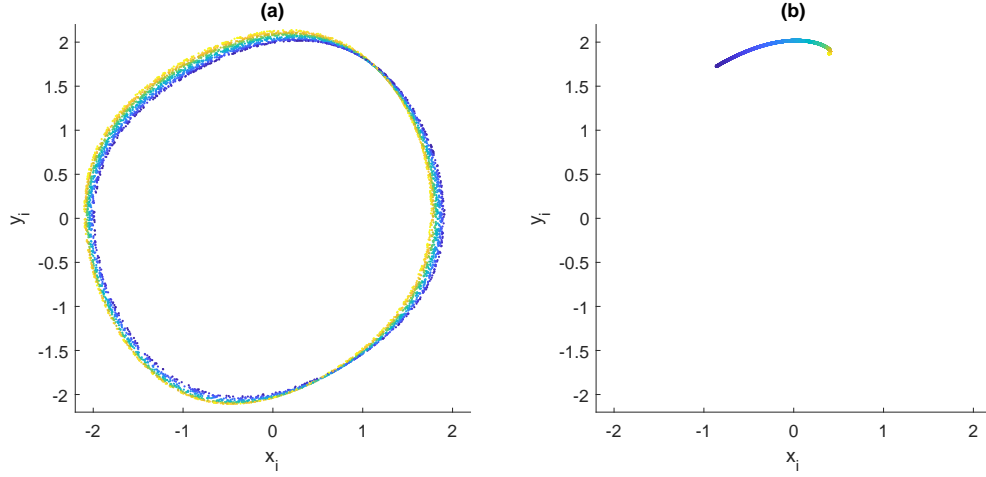
FIG. 13. Snapshot of a stable chimera solution of (55)-(59). The oscillators are coloured by their b_i value (blue low, yellow high). (a): population 1; (b): population 2. Parameters: $\mu = 0.09, \nu = 0.01, \epsilon = 0.2, c = 0.1, b_0 = 1, \Delta b = 0.7, N = 5000$.

for $i = N + 1, \ldots 2N$, where

$$\bar{X}_1 = \frac{1}{N}\sum_{i=1}^{N} x_i; \qquad \bar{Y}_1 = \frac{1}{N}\sum_{i=1}^{N} y_i; \qquad \bar{X}_2 = \frac{1}{N}\sum_{i=1}^{N} x_{N+i}; \qquad \bar{Y}_2 = \frac{1}{N}\sum_{i=1}^{N} y_{N+i} \tag{59}$$

As usual, μ is the within-population coupling strength and ν is the between-population strength. There is mean-field coupling involving both x and y variables. Equations of this form were considered in [4, 12] although with nonlocal coupling on a ring of oscillators. We set $\epsilon = 0.2, \mu = 0.09, \nu = 0.01, c = 0.1$ and consider heterogeneity in the b_i, choosing them from a uniform distribution on $[b_0 - \Delta b, b_0 + \Delta b]$. An example of a stable chimera for $b_0 = 1, \Delta b = 0.7$ is shown in Fig. 13. Population 1 is incoherent while population 2 is synchronised. For population 1 it is clear that oscillators with different b_i lie on different curves.

To analyse this state suppose population 2 is synchronised and $x_{N+i} = X_i$ and $y_{N+i} = Y_i$ for $i = 1, 2 \ldots N$. These are the values shown in Fig. 13(b). Then we have

$$\frac{dX_i}{dt} = Y_i \tag{60}$$

$$\frac{dY_i}{dt} = \epsilon(1 - X_i^2)Y_i - X_i + \mu[b_i(\bar{X}_2 - X_i) + c(\bar{Y}_2 - Y_i)] + \nu[b_i(\bar{X}_1 - X_i) + c(\bar{Y}_1 - Y_i)] \tag{61}$$

For population 1, we see from Fig. 13(a) that oscillators lie on curves which completely contain the origin, so moving to polar coordinates by writing $r_i^2 = x_i^2 + y_i^2$ and $\tan\theta_i = y_i/x_i$ so that $x_i = r_i\cos\theta_i$ and $y_i = r_i\sin\theta_i$ we have

$$\frac{dr_i}{dt} = \frac{x_i\frac{dx_i}{dt} + y_i\frac{dy_i}{dt}}{r_i} \equiv F(r_i, \theta_i, \bar{X}_1, \bar{Y}_1, \bar{X}_2, \bar{Y}_2, b_i) \tag{62}$$

$$\frac{d\theta_i}{dt} = \frac{x_i\frac{dy_i}{dt} - y_i\frac{dx_i}{dt}}{r_i^2} \equiv G(r_i, \theta_i, \bar{X}_1, \bar{Y}_1, \bar{X}_2, \bar{Y}_2, b_i) \tag{63}$$

where dx_i/dt and dy_i/dt are given by (55)-(56). Taking the continuum limit we consider the dynamical system

$$\frac{\partial R}{\partial t}(\theta, t; b) = F(R, \theta, \bar{X}_1, \bar{Y}_1, \bar{X}_2, \bar{Y}_2, b) - G(R, \theta, \bar{X}_1, \bar{Y}_1, \bar{X}_2, \bar{Y}_2, b)\frac{\partial R}{\partial \theta} \tag{64}$$

$$\frac{\partial P}{\partial t}(\theta, t; b) = -\frac{\partial}{\partial \theta}\left[P(\theta, t)G(R, \theta, \bar{X}_1, \bar{Y}_1, \bar{X}_2, \bar{Y}_2, b)\right] + D\frac{\partial^2}{\partial \theta^2}P(\theta, t; b) \tag{65}$$

together with

$$\frac{\partial X(b, t)}{\partial t} = Y \tag{66}$$

$$\frac{\partial Y(b, t)}{\partial t} = \epsilon(1 - X^2)Y - X + \mu[b(\bar{X}_2 - X) + c(\bar{Y}_2 - Y)] + \nu[b(\bar{X}_1 - X) + c(\bar{Y}_1 - Y)] \tag{67}$$
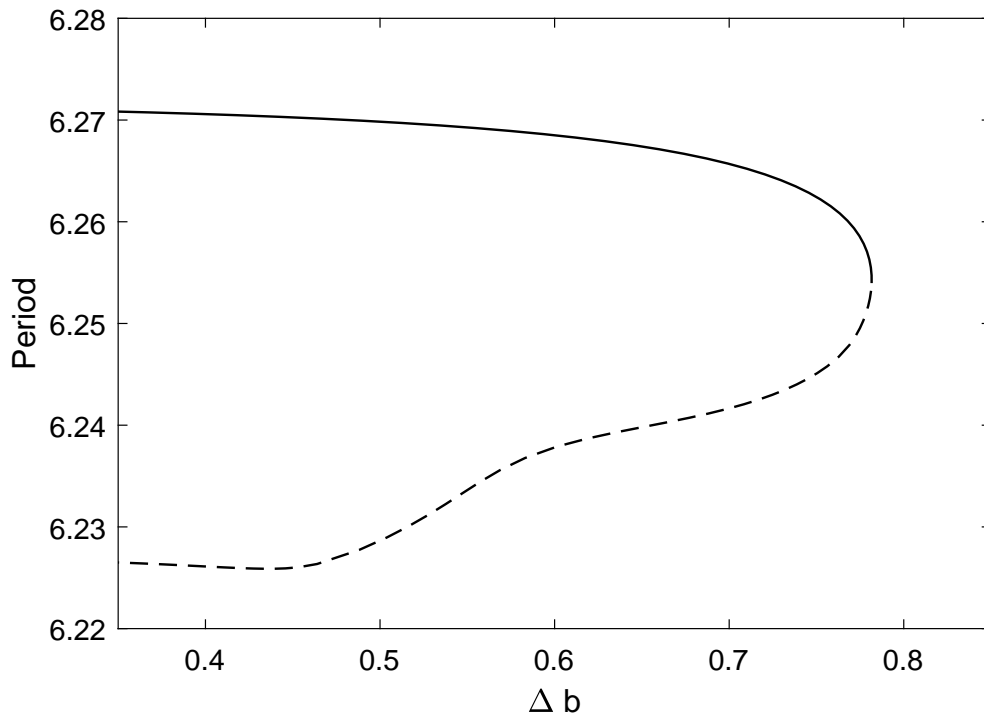
FIG. 14. Period of the periodic chimera solution of (64)-(69). Solid: stable; dashed: unstable. Parameters: $\mu = 0.09, \nu = 0.01, \epsilon = 0.2, c = 0.1, b_0 = 1, D = 10^{-4}$. θ is discretised in 128 points and b in 10.

where

$$\bar{X}_1 = \int_B \int_0^{2\pi} P(\theta, t; b) R(\theta, t; b) \cos\theta \; d\theta \; db; \qquad \bar{Y}_1 = \int_B \int_0^{2\pi} P(\theta, t; b) R(\theta, t; b) \sin\theta \; d\theta \; db \qquad (68)$$

and

$$\bar{X}_2 = \int_B X(b, t) \; db; \qquad \bar{Y}_2 = \int_B Y(b, t) \; db \qquad (69)$$

where B is the interval $[b_0 - \Delta b, b_0 + \Delta b]$.

A significant difference between this system and those in the previous sections is that we cannot go a uniformly rotating coordinate frame in which X and Y are constant. Thus the chimera of interest is a periodic solution of (64)-(69). We numerically continue periodic solutions using pseudo-arclength continuation and determine their stability in terms of the magnitude of the Floquet multipliers of that solution. We obtain Fig. 14, where we see the stable periodic solution is destroyed in a saddle-node bifurcation as Δb is increased. Unlike the systems studied in Secs. II and III, the stable chimera in this system is genuinely stable, without marginal or nearly marginal Floquet multipliers.

VI. DISCUSSION

We have considered chimeras in networks formed from two coupled populations of oscillators. In each network one parameter has been chosen randomly from a uniform distribution. For narrow enough distributions the chimeras which exist for the case of identical parameters persist, and the synchronous oscillators remain synchronised, although no longer having identical states. We generalised the theory in [25] to cover these states, at the price of increased computational effort. In all cases we found that chimeras were destroyed in saddle-node bifurcations as the width of the uniform distribution was increased. We now discuss several generalisations of the approach taken here.

While we have considered heterogeneity in only one parameter at a time, it is possible to consider more than one. As an example, take a network of the form (1)-(2) where not only the ω_j are taken from a uniform distribution on $[\omega_0 - \Delta\omega, \omega_0 + \Delta\omega]$ but the values of ν are taken from a uniform distribution on $[\nu_0 - \Delta\nu, \nu_0 + \Delta\nu]$, as considered in Sec. II B. A snapshot of a stable chimera state for such a network is shown in Fig. 15. We see that population 1
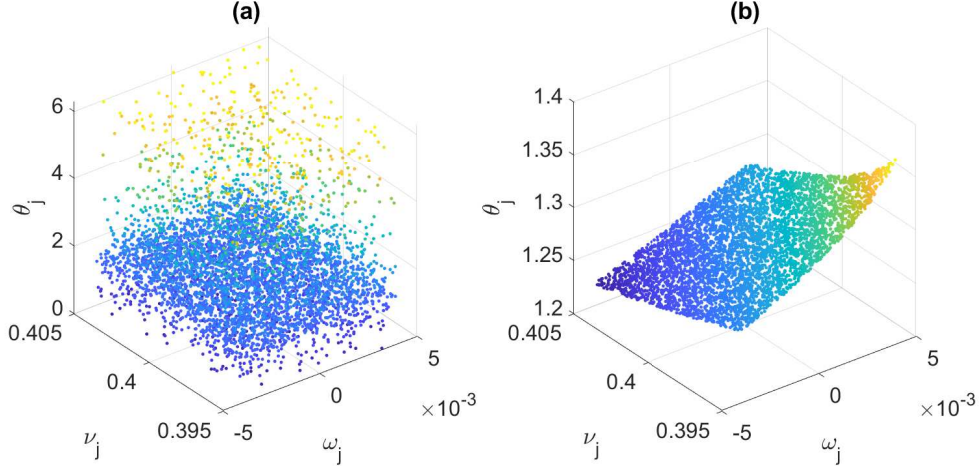
FIG. 15. Snapshot of a chimera state for a network of the form (1)-(2). (a): population 1; (b): population 2. The colour shows the values of the θ_j, with different ranges in the two panels. Parameters: $\mu = 0.6, \nu_0 = 0.4, \Delta\nu = 0.005, \omega_0 = 0, \Delta\omega = 0.004, \beta = 0.08, N = 5000$.

is incoherent while population 2 is locked. In the continuum limit the state of oscillators in population 2 could be described by a function $\phi(\omega, \nu, t)$ defined for $(\omega, \nu) \in [\omega_0 - \Delta\omega, \omega_0 + \Delta\omega] \times [\nu_0 - \Delta\nu, \nu_0 + \Delta\nu]$, while those in population 1 would be described by a complex-valued function $a(\omega, \nu, t)$ defined for the same range of (ω, ν). Numerical studies of such systems would be more involved than the study of networks with a single heterogeneous parameter.

Another possibility is to consider nontrivial connectivity within or between populations. For example, we could replace (1) by

$$\frac{d\theta_j}{dt} = \omega + \frac{\mu}{N} \sum_{k=1}^{N} \sin(\theta_k - \theta_j - \alpha) + \frac{\nu}{\langle d \rangle} \sum_{k=1}^{N} A_{jk} \sin(\theta_{N+k} - \theta_j - \alpha) \tag{70}$$

and similarly for (2) where A is the connectivity matrix between populations: $A_{jk} = 1$ if oscillator k in one population is connected to oscillator j in the other and $A_{jk} = 0$ otherwise. (Connections are undirected, so A is symmetric.) $\langle d \rangle$ the mean degree: $\langle d \rangle = \sum_{j,k} A_{jk}/N$. If the connections between networks are made randomly and each oscillator is connected to sufficiently many others we can make the approximation [53]

$$\frac{1}{\langle d \rangle} \sum_{k=1}^{N} A_{jk} \sin(\theta_{N+k} - \theta_j - \alpha) \approx \frac{d_j}{N \langle d \rangle} \sum_{k=1}^{N} \sin(\theta_{N+k} - \theta_j - \alpha) \tag{71}$$

where d_j is the degree of oscillator j: $d_j \equiv \sum_{k=1}^{N} A_{jk}$. Thus having a range of degrees has approximately the same effect on the dynamics as having a range of ν values, as investigated in Sec. II B. To compare with the results in Sec. II B we construct networks using the configuration model [54] having degree distributions which are uniform on $[d_0 - \Delta d, d_0 + \Delta d]$ and set $\nu = 0.4$. The corresponding value of $\Delta\nu$ as shown in Fig. 5 is $\Delta\nu = \nu(\Delta d/d_0) = 0.4(\Delta d/d_0)$, but note that both Δd and d_0 are integers.

We construct networks with $N = 5000$ and d_0 either 1000 or 2000, and numerically solve equations of the form (70) with initial conditions close to a chimera state. We define the real order parameter for the synchronised (or largely synchronised) population

$$R = \left| \frac{1}{N} \sum_{j=1}^{N} e^{i\theta_j} \right| \tag{72}$$

and (after transients) measure the standard deviation of R over 300 time units. This standard deviation is plotted on a log scale in Fig. 16 as a function of $0.4(\Delta d/d_0)$ for the two different values of d_0. We see a rapid increase in the standard deviation indicating the loss of full synchrony of the synchronised population when $0.4(\Delta d/d_0)$ is approximately 0.011-0.012, in very good agreement with Fig. 5. Note that several other authors have studied chimeras in a pair of subnetworks with less than all-to-all connectivity [55–57].
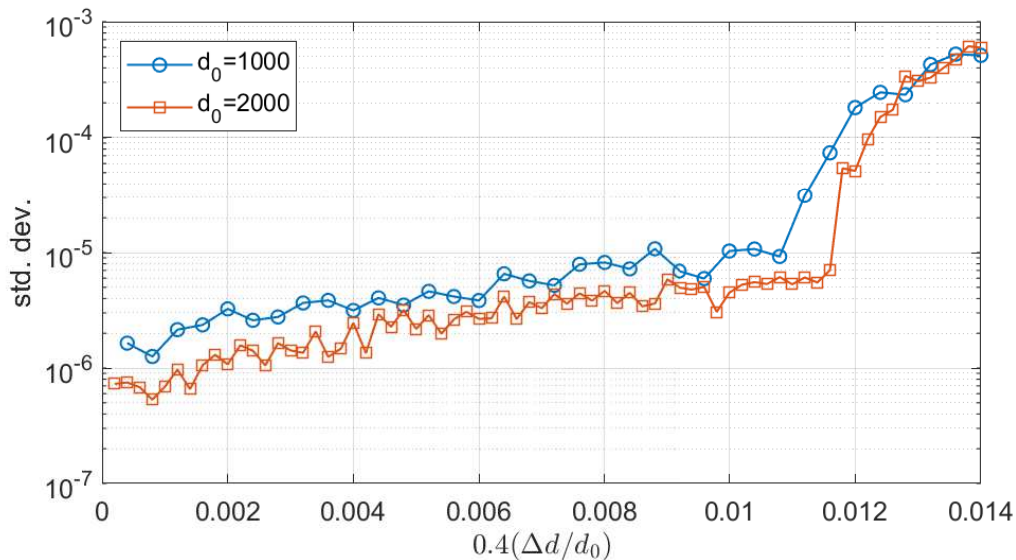
FIG. 16. Standard deviation of the order parameter (72) as a function of the width of the degree distribution, Δd. Parameters: $\mu = 0.6, \nu = 0.4, \omega = 0, \beta = 0.08, N = 5000$.

All of the results shown here have used a uniform distribution of heterogeneous parameters, so to confirm the validity of these results we also considered a beta distribution with equal shape parameters. For a beta distribution the distribution of a parameter x with non-zero density on $[x_0 - \Delta x, x_0 + \Delta x]$ is proportional to

$$p(x) = \left(1 - \frac{x - x_0}{\Delta x}\right)^{\alpha} \left(1 + \frac{x - x_0}{\Delta x}\right)^{\alpha} \tag{73}$$

where α is the shape parameter. Integrals over x are then approximated using Gauss-Gegenbauer quadrature [58]. We set $\alpha = 2$ and used a discretisation of 10 points. All of the results presented above for a uniform distribution were qualitatively reproduced using this beta distribution (not shown).

Although we considered networks with all-to-all connectivity within and between populations, the governing equations were derived in the continuum limit. Thus the dynamics of large but finite networks whose graphs have the same graphon (or graph limit) [59] as the networks studied here, of the form

$$W(x, y) = \begin{cases} a, & (x, y) \in [0, 1/2] \times [0, 1/2] \text{ or } (x, y) \in [1/2, 1] \times [1/2, 1] \\ b, & \text{otherwise} \end{cases} \tag{74}$$

where a and b are constants with $b < a$ should also be described using the techniques presented here, under the assumption that a parameter is uniformly distributed. Examples include Erdös-Rényi networks, where the probability of connecting two oscillators within or between populations is constant (but less than 1) and Paley graphs [60].

It might seem possible to generalise the techniques presented here to study chimeras on rings of nonlocally coupled general oscillators [4, 16]. However, while the locked oscillators would be described by ODEs and the asynchronous ones by PDEs, one would need to know (or to automatically find) the boundaries between such groups of oscillators, in order to determine whether an ODE or a PDE was needed to describe the dynamics at a particular position on the ring. Also, these boundary points would move as parameters were varied.

---

[1] Mark J Panaggio and Daniel M Abrams. Chimera states: coexistence of coherence and incoherence in networks of coupled oscillators. *Nonlinearity*, 28(3):R67, 2015.

[2] O E Omel'chenko. The mathematics behind chimera states. *Nonlinearity*, 31(5):R121–R164, apr 2018.

[3] Daniel M. Abrams and Steven H. Strogatz. Chimera states in a ring of nonlocally coupled oscillators. *Int. J. Bifn. Chaos*, 16:21–37, 2006.

[4] Iryna Omelchenko, Anna Zakharova, Philipp Hövel, Julien Siebert, and Eckehard Schöll. Nonlinearity of local dynamics promotes multi-chimeras. *Chaos: An Interdisciplinary Journal of Nonlinear Science*, 25(8):083104, 2015.

[5] Carlo R Laing. Chimeras in two-dimensional domains: heterogeneity and the continuum limit. *SIAM Journal on Applied Dynamical Systems*, 16(2):974–1014, 2017.

[6] Mark J Panaggio and Daniel M Abrams. Chimera states on the surface of a sphere. *Physical Review E*, 91(2):022909, 2015.

[7] Daniel M. Abrams, Rennie Mirollo, Steven H. Strogatz, and Daniel A. Wiley. Solvable model for chimera states of coupled oscillators. *Phys. Rev. Lett.*, 101:084103, 2008.

[8] Arkady Pikovsky and Michael Rosenblum. Partially integrable dynamics of hierarchical populations of coupled oscillators. *Phys. Rev. Lett.*, 101:264103, 2008.

[9] Mark J Panaggio, Daniel M Abrams, Peter Ashwin, and Carlo R Laing. Chimera states in networks of phase oscillators: the case of two small populations. *Physical Review E*, 93(1):012218, 2016.

[10] Y. Kuramoto and D. Battogtokh. Coexistence of Coherence and Incoherence in Nonlocally Coupled Phase Oscillators. *Nonlinear Phenom. Complex Syst.*, 5:380–385, 2002.

[11] Carlo R Laing. Chimeras in networks of planar oscillators. *Physical Review E*, 81(6):066221, 2010.

[12] Stefan Ulonska, Iryna Omelchenko, Anna Zakharova, and Eckehard Schöll. Chimera states in networks of van der pol oscillators with hierarchical connectivities. *Chaos: An Interdisciplinary Journal of Nonlinear Science*, 26(9):094825, 2016.

[13] Tassos Bountis, Vasileios G Kanas, Johanne Hizanidis, and Anastasios Bezerianos. Chimera states in a two–population network of coupled pendulum–like elements. *The European Physical Journal Special Topics*, 223(4):721–728, 2014.

[14] Simona Olmi. Chimera states in coupled kuramoto oscillators with inertia. *Chaos: An Interdisciplinary Journal of Nonlinear Science*, 25(12):123125, 2015.

[15] Simona Olmi, Antonio Politi, and Alessandro Torcini. Collective chaos in pulse-coupled neural networks. *EPL (Europhysics Letters)*, 92(6):60007, 2011.

[16] Iryna Omelchenko, Oleh E. Omel'chenko, Philipp Hövel, and Eckehard Schöll. When nonlocal coupling between oscillators becomes stronger: Patched synchrony or multichimera states. *Phys. Rev. Lett.*, 110:224101, May 2013.

[17] Irmantas Ratas and Kestutis Pyragas. Symmetry breaking in two interacting populations of quadratic integrate-and-fire neurons. *Phys. Rev. E*, 96:042212, Oct 2017.

[18] Anna Zakharova, Marie Kapeller, and Eckehard Schöll. Amplitude chimeras and chimera death in dynamical networks. *Journal of Physics: Conference Series*, 727:012018, jun 2016.

[19] Matthias Wolfrum and Oleh Omel'chenko. Chimera states are chaotic transients. *Physical Review E*, 84(1):015201, 2011.

[20] S. Shima and Y. Kuramoto. Rotating spiral waves with phase-randomized core in nonlocally coupled oscillators. *Physical Review E*, 69(3):036213, 2004.

[21] Daniel M. Abrams and Steven H. Strogatz. Chimera states for coupled oscillators. *Phys. Rev. Lett.*, 93:174102, 2004.

[22] Edward Ott and Thomas M. Antonsen. Low dimensional behavior of large systems of globally coupled oscillators. *Chaos*, 18:037113, 2008.

[23] Edward Ott and Thomas M Antonsen. Long time evolution of phase oscillator systems. *Chaos: An interdisciplinary journal of nonlinear science*, 19(2):023117, 2009.

[24] Carlo R Laing. The dynamics of chimera states in heterogeneous kuramoto networks. *Physica D: Nonlinear Phenomena*, 238(16):1569–1588, 2009.

[25] Carlo R Laing. Dynamics and stability of chimera states in two coupled populations of oscillators. *Physical Review E*, 100(4):042211, 2019.

[26] Pau Clusella and Antonio Politi. Between phase and amplitude oscillators. *Phys. Rev. E*, 99:062201, Jun 2019.

[27] Mark R Tinsley, Simbarashe Nkomo, and Kenneth Showalter. Chimera and phase-cluster states in populations of coupled chemical oscillators. *Nature Physics*, 8(9):662, 2012.

[28] Erik Andreas Martens, Shashi Thutupalli, Antoine Fourrière, and Oskar Hallatschek. Chimera states in mechanical oscillator networks. *Proceedings of the National Academy of Sciences USA*, 110(26):10563–10567, 2013.

[29] Jan Frederik Totz, Julian Rode, Mark R Tinsley, Kenneth Showalter, and Harald Engel. Spiral wave chimera states in large populations of coupled chemical oscillators. *Nature Physics*, 14(3):282–285, 2018.

[30] S. Watanabe and SH Strogatz. Constants of motion for superconducting Josephson arrays. *Physica. D*, 74:197–253, 1994.

[31] E. A. Martens, E. Barreto, S. H. Strogatz, E. Ott, P. So, and T. M. Antonsen. Exact results for the kuramoto model with a bimodal frequency distribution. *Physical Review E*, 79:026204, 2009.

[32] Steven H Strogatz and Renato E Mirollo. Stability of incoherence in a population of coupled oscillators. *Journal of Statistical Physics*, 63(3):613–635, 1991.

[33] Kevin M Hannay, Daniel B Forger, and Victoria Booth. Macroscopic models for networks of coupled biological oscillators. *Science advances*, 4(8):e1701047, 2018.

[34] Julio D da Fonseca, Edson D Leonel, and Hugues Chaté. Instantaneous frequencies in the kuramoto model. *Physical Review E*, 102(5):052127, 2020.

[35] Bastian Pietras, Nicolás Deschle, and Andreas Daffertshofer. First-order phase transitions in the kuramoto model with compact bimodal frequency distributions. *Physical Review E*, 98(6):062219, 2018.

[36] Diego Pazó. Thermodynamic limit of the first-order phase transition in the kuramoto model. *Physical Review E*, 72(4):046211, 2005.

[37] Yernur Baibolatov, Michael Rosenblum, Zeinulla Zh Zhanabaev, and Arkady Pikovsky. Complex dynamics of an oscillator ensemble with uniformly distributed natural frequencies and global nonlinear coupling. *Physical Review E*, 82(1):016212, 2010.

[38] Bertrand Ottino-Löffler and Steven H. Strogatz. Kuramoto model with uniformly spaced frequencies: Finite-n asymptotics of the locking threshold. *Phys. Rev. E*, 93:062220, Jun 2016.

[39] Sebastian Eydam and Matthias Wolfrum. Mode locking in systems of globally coupled phase oscillators. *Phys. Rev. E*, 96:052205, Nov 2017.

[40] G Bard Ermentrout. Synchronization in a pool of mutually coupled oscillators with random frequencies. *Journal of Mathematical Biology*, 22(1):1–9, 1985.

[41] EV Rybalova, TE Vadivasova, GI Strelkova, Vadim S Anishchenko, and AS Zakharova. Forced synchronization of a multilayer heterogeneous network of chaotic maps in the chimera state mode. *Chaos: An Interdisciplinary Journal of Nonlinear Science*, 29(3):033134, 2019.

[42] Carlo R. Laing. Chimera states in heterogeneous networks. *Chaos*, 19:013113, 2009.

[43] Ernest Montbrió, Jürgen Kurths, and Bernd Blasius. Synchronization of two interacting populations of oscillators. *Phys. Rev. E*, 70:056125, 2004.

[44] Carlo R. Laing. Numerical bifurcation theory for high-dimensional neural models. *The Journal of Mathematical Neuroscience*, 4(1):1–27, 2014.

[45] Willy JF Govaerts. *Numerical methods for bifurcations of dynamical equilibria*. SIAM, 2000.

[46] G Bard Ermentrout and John Rinzel. Beyond a pacemaker's entrainment limit: phase walk-through. *American Journal of Physiology-Regulatory, Integrative and Comparative Physiology*, 246(1):R102–R106, 1984.

[47] S. Watanabe and S.H. Strogatz. Integrability of a globally coupled oscillator array. *Physical Review Letters*, 70:2391–2394, 1993.

[48] Xiyun Zhang, Hongjie Bi, Shuguang Guan, Jinming Liu, and Zonghua Liu. Model bridging chimera state and explosive synchronization. *Physical Review E*, 94(1):012204, 2016.

[49] Lloyd N Trefethen. *Spectral methods in MATLAB*, volume 10. Siam, 2000.

[50] Bard Ermentrout. Gap junctions destroy persistent states in excitatory networks. *Physical Review E*, 74(3):031918, 2006.

[51] J. Guckenheimer and P. Holmes. *Nonlinear Oscillations, Dynamical Systems, and Bifurcations of Vector Fields*. Springer, 1983.

[52] Y.A. Kuznetsov. *Elements of Applied Bifurcation Theory*. Springer, 2004.

[53] T.W. Ko and G.B. Ermentrout. Partially locked states in coupled oscillators due to inhomogeneous coupling. *Physical Review E*, 78(1):016203, 2008.

[54] Mark EJ Newman. The structure and function of complex networks. *SIAM review*, 45(2):167–256, 2003.

[55] Simona Olmi and Alessandro Torcini. Chimera states in pulse coupled neural networks: the influence of dilution and noise. In *Nonlinear Dynamics in Computational Neuroscience*, pages 65–79. Springer, 2019.

[56] Carlo R Laing, Karthikeyan Rajendran, and Ioannis G Kevrekidis. Chimeras in random non-complete networks of phase oscillators. *Chaos: An Interdisciplinary Journal of Nonlinear Science*, 22(1):013132, 2012.

[57] Bo Li and David Saad. Chimera-like states in structured heterogeneous networks. *Chaos: An Interdisciplinary Journal of Nonlinear Science*, 27(4):043109, 2017.

[58] https://people.sc.fsu.edu/$\sim$ jburkardt/m_src/gegenbauer_rule/gegenbauer_rule.html.

[59] László Lovász and Balázs Szegedy. Limits of dense graph sequences. *Journal of Combinatorial Theory, Series B*, 96(6):933–957, 2006.

[60] Hayato Chiba, Georgi S Medvedev, and Matthew S Mizuhara. Bifurcations in the kuramoto model on graphs. *Chaos: An Interdisciplinary Journal of Nonlinear Science*, 28(7):073109, 2018.